Chapter 2

Linear theory

2.1 Introduction

In this chapter, we will begin our investigations of magnetoconvection in tilted fields by studying the linear stability theory for a simple model problem. Our philosophy will be to create a simplified, idealized model rather than trying to include all the details of the physics. This will allow us to learn something about the problem without over-complicating the calculations or having to do time-consuming numerical simulations. Once we understand the basics, we will then be in a position, in later chapters, to move on to more complicated (and more realistic) models.

With this in mind, we will look at Boussinesq convection in a layer containing a uniform inclined magnetic field. Unlike previous work (Matthews et al., 1992) we do not consider fully compressible convection, although it will turn out that many of the features of the compressible problem are captured in our model. We do, however, consider fully three-dimensional solutions; the work of Matthews et al. (1992) was restricted to two dimensions. This work will give us a rough idea what happens near the onset of convection, and will provide a good starting point for the weakly nonlinear models of the next chapter.

We will first of all, in section 2.2, describe in detail our problem and our method of solving it. In section 2.3 we review what happens when the field is vertical, and in section 2.4 we show how symmetry arguments may be used to ascertain what happens when the field is tilted. Finally, we present our results in section 2.5, and give conclusions in section 2.6.

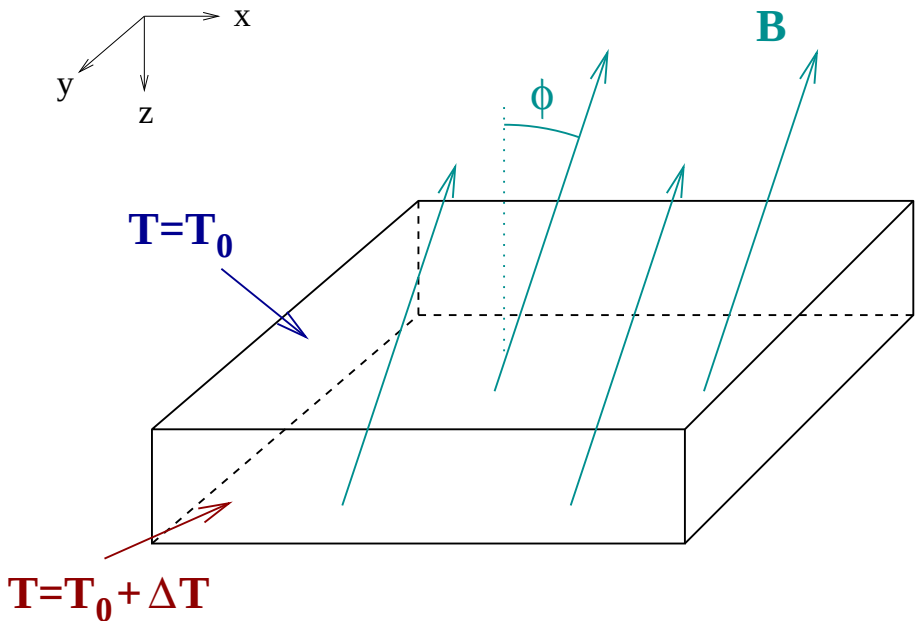

Figure 2.1: *Diagram showing the system under investigation.*

2.2 Problem setup

The problem that we will investigate consists of an infinite horizontal plane layer of Boussinesq fluid, heated from below, and permeated by an inclined magnetic field tilted at an angle ϕ to the vertical. Refer to Figure 2.1.

The equations of motion for the layer, in non-dimensionalized form, are as follows: the Navier–Stokes equation

$$\frac{1}{\sigma}\left(\frac{\partial \boldsymbol{u}}{\partial t} + \boldsymbol{u}\cdot\nabla\boldsymbol{u}\right) = -\nabla\Pi + \frac{d^3}{\nu\bar{\kappa}}\boldsymbol{g} - RT\boldsymbol{e}_z + \zeta Q\boldsymbol{B}\cdot\nabla\boldsymbol{B} + \nabla^2\boldsymbol{u}, \tag{2.1}$$

the temperature equation (where we assume that radiative transfer can be treated in the diffusive approximation)

$$\frac{\partial T}{\partial t} + \boldsymbol{u}\cdot\nabla T = \nabla\cdot(\hat{\kappa}\nabla T), \tag{2.2}$$

and the induction equation

$$\frac{\partial \boldsymbol{B}}{\partial t} + \boldsymbol{u}\cdot\nabla\boldsymbol{B} = \boldsymbol{B}\cdot\nabla\boldsymbol{u} + \zeta\nabla^2\boldsymbol{B}, \tag{2.3}$$

together with

$$\nabla\cdot\boldsymbol{u} = \nabla\cdot\boldsymbol{B} = 0, \tag{2.4}$$

where $\boldsymbol{u}$ is the fluid velocity, $\boldsymbol{B}$ is the magnetic field, T is the temperature, and $\Pi = p + \boldsymbol{B}^2/2\mu_0$ is the total pressure (gas pressure plus magnetic pressure). In these equations

we have scaled all lengths by the layer depth d, times by the thermal diffusion timescale $d^2/\bar{\kappa}$, magnetic fields by the imposed field strength B_0, and temperatures by the imposed temperature difference ΔT. This leaves the following dimensionless parameters: the Rayleigh number R, the Chandrasekhar number Q, the Prandtl number σ and the ratio ζ of magnetic to thermal diffusivity, given by

$$R = \frac{\alpha_T \Delta T d^3 |\boldsymbol{g}|}{\nu \bar{\kappa}}, \qquad Q = \frac{B_0^2 d^2}{\mu_0 \rho \nu \eta}, \qquad \sigma = \frac{\nu}{\bar{\kappa}}, \qquad \zeta = \frac{\eta}{\bar{\kappa}}. \tag{2.5}$$

Here α_T is the coefficient of thermal expansion, $\boldsymbol{g}$ is the acceleration due to gravity, ν is the fluid viscosity, η the magnetic diffusivity, μ_0 the permeability, and ρ the density. The thermal diffusivity of the fluid is denoted by κ; the quantity $\bar{\kappa}$ in the above equations represents the value of κ at mid-layer ($z = 1/2$). Initially we will assume that κ is a constant (so that $\kappa = \bar{\kappa}$ everywhere), but later on we will allow for the possibility of a varying thermal diffusivity with depth. In this case we write κ as

$$\kappa = \hat{\kappa}(z)\bar{\kappa}, \tag{2.6}$$

where $\hat{\kappa}$ is a dimensionless function of depth. (For consistency, $\hat{\kappa}$ must satisfy $\hat{\kappa}(1/2) = 1$.)

2.2.1 Boundary conditions

We must also specify boundary conditions for our layer. We will assume that our layer is of infinite extent in the horizontal, so we only need to specify boundary conditions for the top and bottom surfaces. We take these surfaces to be impenetrable and stress free, so that

$$u_z = \frac{\partial u_x}{\partial z} = \frac{\partial u_y}{\partial z} = 0 \tag{2.7}$$

at $z = 0$ and at $z = 1$. We also take the temperature to be fixed at top and bottom, which in the non-dimensional units adopted, reduces to

$$T = 0 \text{ at } z = 0; \quad T = 1 \text{ at } z = 1. \tag{2.8}$$

This leaves the question of what to do with the magnetic boundary conditions. There are actually several plausible choices. The simplest would be to fix the angle of the magnetic field at the top and bottom surfaces, so that

$$B_x = -B_z \tan\phi; \quad B_y = 0 \tag{2.9}$$

on the boundary. However this is not physically realistic and can in some circumstances lead to energy being injected into the system from the boundaries (N.Roxburgh, private communication).

Instead, there are two physically motivated boundary conditions that we could use: we could take the boundary to be either a perfect electrical insulator or a perfect electrical conductor. The former is equivalent to matching to a potential field outside the layer, while the latter is equivalent to 'tying' the field lines (and in 2D it is also equivalent to holding the vector potential fixed at its initial value). We derive equations for these conditions in Appendix A. Although still somewhat idealized, these conditions are slightly more realistic than simply fixing the tilt angle.

For example, in the Sun we can to a first approximation assume that there is a vacuum (or at least, a current-free region) above the surface, so it is reasonable to match our solution onto a potential field above the top of the layer. We take the potential field to be inclined at an angle ϕ as $z \to -\infty$ (which is how the inclination of the field is controlled).

Below the layer, matching to a potential field is inappropriate. Instead, we take a perfectly conducting lower boundary, which 'ties' the footpoints of the field lines in place. (This seems reasonable if we think of the field in a sunspot as being anchored to a flux tube which is deeply rooted near the base of the convection zone.)

2.2.2 Basic state and linearization

The equations given above have a trivial solution in which the fluid velocity is zero and the magnetic field is uniform: $\boldsymbol{B} = \boldsymbol{B}_0 \equiv (-\sin\phi, 0, \cos\phi)$ in non-dimensional units. The temperature profile is linear if κ is uniform; if κ varies with depth, it is instead given by

$$T = T_0(z) \equiv C \int \frac{1}{\hat{\kappa}} dz + D \tag{2.10}$$

where C and D are constants of integration, chosen to ensure that the boundary conditions ($T = 0$ at $z = 0$, $T = 1$ at $z = 1$) are satisfied.

We now wish to analyse the stability of this basic state. The problem is separable

in x, y and t, so we introduce perturbations of the form

$$\boldsymbol{u} = \boldsymbol{u}'(z)\mathrm{e}^{\mathrm{i}\boldsymbol{k}\cdot\boldsymbol{x}+st} + \text{c.c.} \tag{2.11}$$

$$\boldsymbol{B} = \boldsymbol{B}_0 + \boldsymbol{B}'(z)\mathrm{e}^{\mathrm{i}\boldsymbol{k}\cdot\boldsymbol{x}+st} + \text{c.c.} \tag{2.12}$$

$$T = T_0(z) + T'(z)\mathrm{e}^{\mathrm{i}\boldsymbol{k}\cdot\boldsymbol{x}+st} + \text{c.c.} \tag{2.13}$$

$$\Pi = \Pi_0 + \Pi'(z)\mathrm{e}^{\mathrm{i}\boldsymbol{k}\cdot\boldsymbol{x}+st} + \text{c.c.} \tag{2.14}$$

(where 'c.c.' stands for 'complex conjugate'). The vector $\boldsymbol{k}$ is the wavevector of the disturbance, which we also write in components as $\boldsymbol{k} = (k_x, k_y, 0)$.

Choosing the perturbations in this form essentially corresponds to considering one Fourier mode at a time. (Obviously in linear theory different Fourier modes will just superpose, so it is valid to consider them each individually.)

After linearizing in the perturbations, and writing the equations out in components, the following eigenvalue problem for the growth rate s is obtained:

$$\frac{s}{\sigma}u_x' = -\mathrm{i}k_x\Pi' + \zeta Q\left(-\mathrm{i}k_x\sin\phi B_x' + \cos\phi\frac{\mathrm{d}B_x'}{\mathrm{d}z}\right) - (k_x^2+k_y^2)u_x' + \frac{\mathrm{d}^2u_x'}{\mathrm{d}z^2} \tag{2.15}$$

$$\frac{s}{\sigma}u_y' = -\mathrm{i}k_y\Pi' + \zeta Q\left(-\mathrm{i}k_x\sin\phi B_y' + \cos\phi\frac{\mathrm{d}B_y'}{\mathrm{d}z}\right) - (k_x^2+k_y^2)u_y' + \frac{\mathrm{d}^2u_y'}{\mathrm{d}z^2} \tag{2.16}$$

$$\frac{s}{\sigma}u_z' = -\frac{\mathrm{d}\Pi'}{\mathrm{d}z} + \zeta Q\left(-\mathrm{i}k_x\sin\phi B_z' + \cos\phi\frac{\mathrm{d}B_z'}{\mathrm{d}z}\right) - (k_x^2+k_y^2)u_z' + \frac{\mathrm{d}^2u_z'}{\mathrm{d}z^2} - RT' \tag{2.17}$$

$$sT' + \frac{C}{\hat{\kappa}}u_z' = -\hat{\kappa}(k_x^2+k_y^2)T' + \hat{\kappa}\frac{\mathrm{d}^2T'}{\mathrm{d}z^2} + \frac{\mathrm{d}\hat{\kappa}}{\mathrm{d}z}\frac{\mathrm{d}T'}{\mathrm{d}z} \tag{2.18}$$

$$sB_x' = -\mathrm{i}k_x\sin\phi u_x' + \cos\phi\frac{\mathrm{d}u_x'}{\mathrm{d}z} - \zeta(k_x^2+k_y^2)B_x' + \zeta\frac{\mathrm{d}^2B_x'}{\mathrm{d}z^2} \tag{2.19}$$

$$sB_y' = -\mathrm{i}k_x\sin\phi u_y' + \cos\phi\frac{\mathrm{d}u_y'}{\mathrm{d}z} - \zeta(k_x^2+k_y^2)B_y' + \zeta\frac{\mathrm{d}^2B_y'}{\mathrm{d}z^2} \tag{2.20}$$

$$sB_z' = -\mathrm{i}k_x\sin\phi u_z' + \cos\phi\frac{\mathrm{d}u_z'}{\mathrm{d}z} - \zeta(k_x^2+k_y^2)B_z' + \zeta\frac{\mathrm{d}^2B_z'}{\mathrm{d}z^2} \tag{2.21}$$

$$\mathrm{i}k_xu_x' + \mathrm{i}k_yu_y' + \frac{\mathrm{d}u_z'}{\mathrm{d}z} = 0 \tag{2.22}$$

$$\mathrm{i}k_xB_x' + \mathrm{i}k_yB_y' + \frac{\mathrm{d}B_z'}{\mathrm{d}z} = 0 \tag{2.23}$$

subject to

$$u_z' = \frac{\mathrm{d}u_x'}{\mathrm{d}z} = \frac{\mathrm{d}u_y'}{\mathrm{d}z} = T' = 0 \tag{2.24}$$

at both top and bottom.

If the fixed-angle boundary condition is being used for the magnetic field, then the relevant linearized boundary condition is

$$B'_x = -B'_z \tan\phi \tag{2.25}$$

$$B'_y = 0, \tag{2.26}$$

to be applied at $z = 0$ and $z = 1$.

The potential field boundary condition (at $z = 0$) is

$$B'_x = \frac{\mathrm{i}k_x}{\sqrt{k_x^2 + k_y^2}} B'_z \tag{2.27}$$

$$B'_y = \frac{\mathrm{i}k_y}{\sqrt{k_x^2 + k_y^2}} B'_z. \tag{2.28}$$

The (linearized) tied field boundary condition (at $z = 1$) is

$$\zeta \frac{\mathrm{d}B'_x}{\mathrm{d}z} + u'_x \cos\phi - \zeta \mathrm{i}k_x B'_z = 0 \tag{2.29}$$

$$\zeta \frac{\mathrm{d}B'_y}{\mathrm{d}z} + u'_y \cos\phi - \zeta \mathrm{i}k_y B'_z = 0 \tag{2.30}$$

These equations were solved numerically using the program NRK, an implementation of the Newton-Raphson-Kantorovich method for solving boundary value problems (Cash and Moore, 1980). The eigenvalue s can be found in terms of the various parameters. Alternatively the critical Rayleigh number R_c for the onset of instability (at which $\mathrm{Re}\, s = 0$) can be calculated.

2.3 The vertical field case

Before moving on to inclined fields, it is important to understand the case of a vertical field. Here, the layer is isotropic (that is to say, there is rotational symmetry about the z-axis), so without loss of generality we can consider only the two-dimensional problem, taking $k_y = 0$. (We also take k_x to be positive, again without loss of generality.) The isotropy implies a symmetry between leftward- and rightward-travelling waves, which means that the eigenvalues s will always be either purely real (representing steady convection), or come in complex conjugate pairs (representing waves travelling in either direction).

In the Boussinesq case, this problem has been investigated by Chandrasekhar (1961) and Proctor and Weiss (1982). There are two qualitatively different types of behaviour,

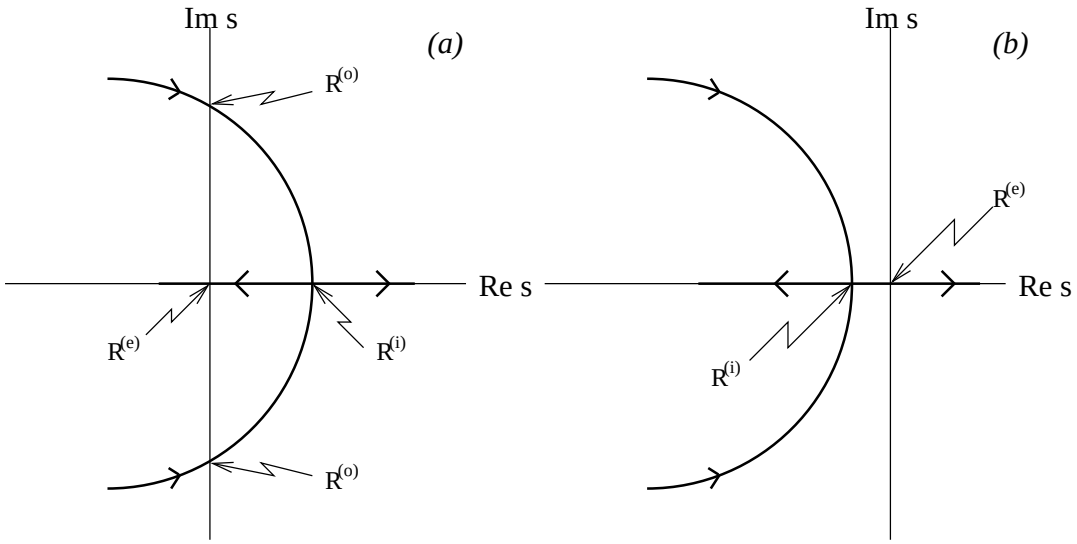

Figure 2.2: *The paths of the eigenvalues through the complex plane as R is varied, when the field is vertical. (a) Oscillatory case (small ζ); (b) steady case (large ζ). (After Proctor and Weiss 1982, figure 6.)*

depending on ζ. The first is the 'oscillatory' case which occurs for $\zeta < 1$ and Q sufficiently large. The second type of behaviour is the 'steady' case and this occurs when $\zeta \geq 1$ or when Q is small enough.

Note that these conditions apply for uniform κ; when κ is non-uniform, there is a slight complication, since the ratio η/κ is now effectively a function of depth. The cut-off between the two types of behaviour will no longer be exactly at $\zeta = 1$; however, we can still say that the oscillatory case occurs for ζ small enough, and the steady case occurs for ζ large enough.

Figure 2.2 shows how the eigenvalues s move through the complex plane as R is increased, in both the oscillatory and steady cases. Note that $\mathrm{Re}\, s$ corresponds to the growth rate (positive indicating instability), while $\mathrm{Im}\, s$ gives the oscillation frequency of the mode. Since we are taking k_x to be positive, we have that $\mathrm{Im}\, s < 0$ represents a rightward-travelling wave, $\mathrm{Im}\, s > 0$ represents a leftward-travelling wave, and $\mathrm{Im}\, s = 0$ indicates a steady mode.

Figure 2.2(a) shows the oscillatory case; various special Rayleigh numbers are marked. $R = R^{(o)}$ corresponds to a Hopf bifurcation, where the static state loses stability to oscillatory convection. $R = R^{(i)}$ represents a transition from oscillatory to steady convection. $R = R^{(e)}$ is where one of the eigenvalues becomes negative again, but this has no physical significance since we are still unstable to the other (positive) eigenvalue.

The steady case is illustrated in Figure 2.2(b). There is now a bifurcation to steady convection at $R = R^{(e)}$, and this time it is $R^{(i)}$ that has no physical significance. Note that the eigenvalues in the right half-plane never leave the real axis, so there is no instability to travelling waves this time.

2.4 Symmetry considerations for inclined fields

We can gain some insight into the inclined field case ($\phi > 0$) by considering the symmetries involved. One important symmetry has already been mentioned, and that is the rotational symmetry present when the field is vertical. When the field is inclined, this symmetry will be broken, and rolls of different orientations will have different properties. We can no longer take $k_y = 0$ and must instead consider the wavenumber to be a two-dimensional vector. Nevertheless, it will be helpful to first consider the 'two-dimensional' case (with $k_y = 0$), in order to explain the various ideas in a simpler setting, before moving on to fully three-dimensional solutions.

2.4.1 General considerations in the two-dimensional case ($k_y = 0$)

Here, we have seen that the isotropy (present for vertical fields) manifests itself as a symmetry between left- and right-going waves, meaning that the eigenvalues come in complex conjugate pairs. When the field is tilted, one would expect this left-right symmetry to be broken. However, for Boussinesq convection this is not the case; this is because there is actually an extra symmetry in the problem.

This extra symmetry is an *up-down* reflection symmetry, inherent in the Boussinesq equations. In our problem, we need to clarify what this means; we are not talking about a simple reflection $z \to -z$, since this would reverse the tilt of the field lines. Instead there is a symmetry π consisting of a reflection in the mid-plane ($z \to -z$) followed by another reflection in the y–z plane ($x \to -x$). (π is equivalent to a 180° rotation, in effect turning the layer 'upside-down'.)

This symmetry transforms a left-going wave into a right-going wave, and vice versa. In other words, the presence of an up-down symmetry also implies that there is a symmetry between left-going and right-going waves, even when the field is tilted.

Contrast this to compressible convection, in which there is no up-down symmetry,

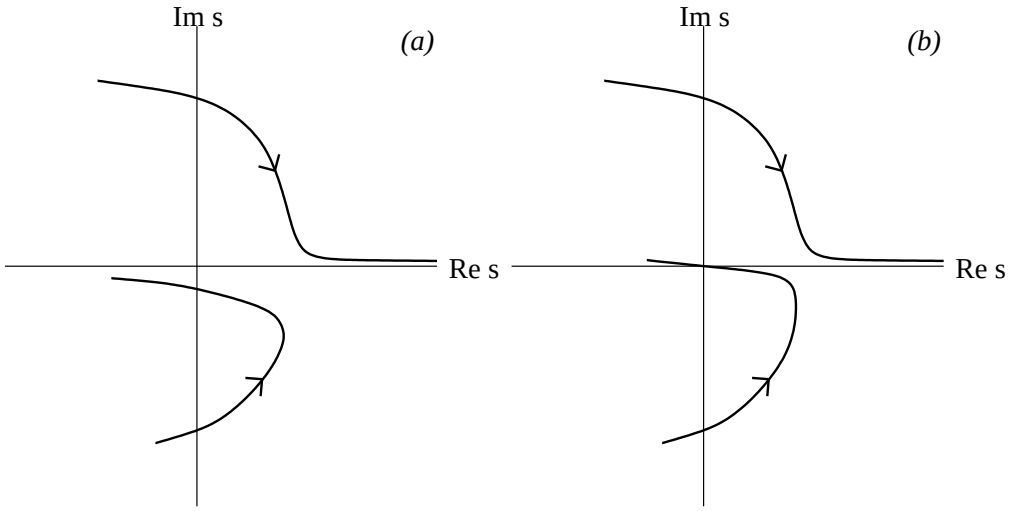

Figure 2.3: *Perturbations to Figure 2.2(a) after breaking the left-right symmetry. (a) The general case. (b) The case where the up-down symmetry is broken only by a change in the magnetic boundary conditions between top and bottom; in this case, the curve must pass through the origin.*

and therefore tilting the field *would* break the symmetry between left-going and right-going waves. Since we are trying to model sunspots, where compressibility is important, it is clearly unsatisfactory that the left-right symmetry is *not* broken in our model.

We are therefore motivated to look for ways in which this symmetry can be broken within our Boussinesq model. First of all, note that one way of achieving this would be to choose different boundary conditions at the top and bottom boundaries. In fact, we have already suggested that an appropriate choice of magnetic boundary conditions would be to use an insulating upper boundary, but a conducting lower boundary. This in itself should be sufficient to break the up-down symmetry.

We will see later on, however, that the approach of breaking the symmetry purely by changing the magnetic boundary conditions is not entirely satisfactory. An alternative method is to allow the thermal diffusivity κ to vary with depth – a possibility that we allowed for when we formulated the equations. This approach allows us to break the symmetry in a somewhat more fundamental way than simply by tweaking the boundary conditions.

We now turn to the changes that we would expect to see in Figure 2.2 when the field is tilted (assuming that the up-down symmetry in the problem has indeed been broken). The main change is that we would expect either left-going waves to be preferred over right-going ones, or vice versa (we cannot say in advance which way around it will be).

We now consider how this works in more detail, starting with the oscillatory case (low ζ) and then moving on to the steady case (high ζ).

2.4.2 The oscillatory case (small ζ)

Here, we wish to describe how Figure 2.2(a), which applies to oscillatory convection when $\phi = 0$, will change when ϕ is increased above zero. Here we are considering the case where the left-right symmetry has been broken (as discussed above); suppose that it is the left-going waves that are preferred. This would shift the top half of the diagram (representing left-going waves) to the right (i.e. becoming more unstable), while the bottom half would be shifted to the left. Thus, we might expect to see a picture something like Figure 2.3(a). (The other possibility, in which right-going waves are preferred, would correspond to a reflection of this figure about the real axis.)

For this result, however, it is important to consider *how* the symmetry π was broken. If this was done solely by changing the magnetic boundary conditions at top and bottom, then we must consider a result of Roberts (1967, p.200), who has shown that when $s = 0$, the magnetic boundary conditions actually have no effect on the problem. That is, if $s = 0$ at $R = R^{(e)}$ for the symmetric problem, then s will still be zero, at the same Rayleigh number, when the magnetic boundary conditions are changed. This is equivalent to saying that the locus of our eigenvalues must still pass through the origin, at the same value of R – although there is nothing to stop it from being perturbed from its original path elsewhere (where $s \neq 0$). Figure 2.3(b) shows the revised picture.

Note that Roberts (1967) only derives this result for the two-dimensional case, but it is a simple matter to extend it to the three-dimensional case (i.e. when $k_y \neq 0$). Following Proctor and Weiss (1982), section 5, we can write the linearized equations in a poloidal-toroidal form. First of all, take the curl of the momentum and induction equations to obtain:

$$\frac{1}{\sigma}\frac{\partial \boldsymbol{\omega}}{\partial t} = -R(\nabla T') \wedge \boldsymbol{e}_z + \zeta Q \boldsymbol{B}_0 \cdot \nabla \boldsymbol{j}' + \nabla^2 \boldsymbol{\omega} \tag{2.31}$$

$$\frac{\partial \boldsymbol{j}'}{\partial t} = \boldsymbol{B}_0 \cdot \nabla \boldsymbol{\omega} + \zeta \nabla^2 \boldsymbol{j}' \tag{2.32}$$

where $\boldsymbol{\omega} = \nabla \wedge \boldsymbol{u}$ and $\boldsymbol{j}' = \nabla \wedge \boldsymbol{B}'$.

The z-components of (2.31) and (2.32) decouple, giving a pair of equations for ω_z

and j_z', as follows:

$$\frac{1}{\sigma}\frac{\partial \omega_z}{\partial t} = \zeta Q \boldsymbol{B}_0 \cdot \nabla j_z' + \nabla^2 \omega_z \tag{2.33}$$

$$\frac{\partial j_z'}{\partial t} = \boldsymbol{B}_0 \cdot \nabla \omega_z + \zeta \nabla^2 j_z'. \tag{2.34}$$

(2.33) and (2.34) are the equations for damped Alfvén waves travelling along the $\boldsymbol{B}_0$ direction. Since there is no driving term, the solutions will decay exponentially and j_z' and ω_z may be set to zero.

Because $\nabla \cdot \boldsymbol{u} = \nabla \cdot \boldsymbol{B}' = 0$, we can now introduce a poloidal-toroidal representation for both $\boldsymbol{u}$ and $\boldsymbol{B}'$. In fact, since ω_z and j_z' are both zero, it follows that the toroidal component will be zero and that $\boldsymbol{u}$ and $\boldsymbol{B}'$ will both be purely poloidal. We write them as

$$\boldsymbol{u} = \nabla \wedge (\nabla \wedge (F \boldsymbol{e}_z)) \tag{2.35}$$

$$\boldsymbol{B}' = \nabla \wedge (\nabla \wedge (H \boldsymbol{e}_z)). \tag{2.36}$$

We can then rewrite the linearized momentum, temperature and induction equations in terms of F and H:

$$\frac{1}{\sigma}\frac{\partial}{\partial t}(\nabla^2 F) = RT' + \zeta Q (\boldsymbol{B}_0 \cdot \nabla)\nabla^2 H + \nabla^4 F \tag{2.37}$$

$$\frac{\partial T'}{\partial t} - (\nabla_H^2 F)\left(\frac{\partial T'}{\partial z}\right) = \frac{\mathrm{d}\hat{\kappa}}{\mathrm{d}z}\frac{\mathrm{d}T_0}{\mathrm{d}z} + \hat{\kappa}\nabla^2 T' \tag{2.38}$$

$$\frac{\partial H}{\partial t} = \boldsymbol{B}_0 \cdot \nabla F + \zeta \nabla^2 H. \tag{2.39}$$

Note that (2.37) couples to (2.39) only through $\nabla^2 H$, while (2.38) does not contain H at all. If we look for steady solutions (in which $\partial/\partial t \equiv 0$), we have from (2.39) that

$$\nabla^2 H = -\frac{1}{\zeta}\boldsymbol{B}_0 \cdot \nabla F \tag{2.40}$$

and we can substitute this into (2.37). Note that (2.37) and (2.38) now decouple completely from (2.39). We can solve the former for the temperature and velocity eigenfunctions, *independently* of the magnetic boundary conditions, thus obtaining our critical Rayleigh number R (when $s = 0$); we can then substitute these solutions into (2.39) and find the magnetic field separately. Therefore, we have proved the above claim that when $s = 0$, the magnetic boundary conditions do not influence the value of the critical Rayleigh number.

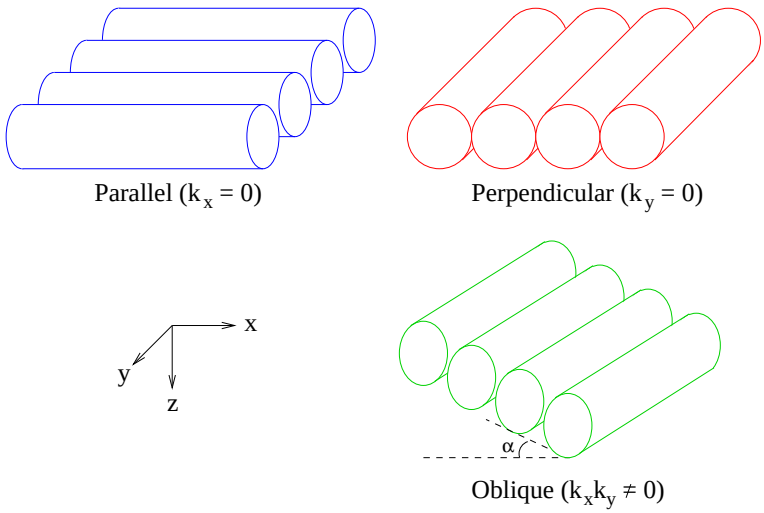

Figure 2.4: *Definitions of 'parallel', 'perpendicular' and 'oblique' rolls. The cylinders in this picture represent the convection rolls. The magnetic field (which is not drawn) lies in the x-z plane.*

The three-dimensional case ($k_y \neq 0$)

We now move on to the general case where k_y can be non-zero. To make things clearer we will introduce an angle α describing the orientation of the wavevector $\boldsymbol{k}$ with respect to the x-axis, defined as follows:

$$k_x = k\cos\alpha, \quad k_y = k\sin\alpha. \tag{2.41}$$

The case $\alpha = 0$ (corresponding to the two-dimensional problem) will be called the 'perpendicular' case (since the roll axes are perpendicular to the plane of the tilt), and $\alpha = 90°$ will be referred to as the 'parallel' case. There are also 'oblique' rolls (with $0° < \alpha < 90°$). These possibilities are illustrated in Figure 2.4.

Rolls of each of these types will have different properties, because of the anisotropy (if $\phi > 0$). As was shown by Matthews et al. (1992), when ϕ is small these modes can be analysed using simple symmetry arguments. We imagine that, for given parameters, we have calculated the critical Rayleigh numbers (minimized over wavenumber) for a vertical field, and we then consider what happens as ϕ is perturbed slightly from zero.

In the case of parallel rolls, the resulting perturbation to R_c is constrained by symmetry. There are two travelling parallel roll modes – one travelling in the positive y direction, the other in the negative y direction – but both of these are equivalent, in the sense that they are related by the $y \to -y$ reflection symmetry, and therefore they both have the same critical Rayleigh number. Moreover, a parallel roll mode is unchanged by

a reflection $x \to -x$ (which changes the sign of ϕ). This implies that ΔR_c for parallel rolls is an *even* function of ϕ; and for small ϕ, it will (generically) be proportional to ϕ^2 at leading order.

Now consider the perpendicular rolls, which are essentially the same as the two-dimensional solutions discussed above. Assuming that we have found a way to break the up-down symmetry in our layer, then, as explained above, there is asymmetry between left- and right-going waves. Therefore, the perturbation to R_c will *not* be an even function of ϕ; it will instead be proportional to ϕ at leading order.

Therefore, we expect the two-dimensional perpendicular mode to be preferred for small ϕ, but for larger ϕ the parallel rolls 'overtake' and become the preferred mode.

Turning to the oblique rolls, we can examine these by using the following simple model equation (from Matthews et al., 1992):

$$\Delta R_c = \pm \phi B \cos\alpha - \phi^2 C \sin^2\alpha, \tag{2.42}$$

where ΔR_c represents the perturbation to the critical Rayleigh number (for small ϕ). This is effectively a way of combining the effects on the parallel and perpendicular rolls into a single equation. We choose $B > 0$ (without loss of generality) and $C > 0$ (because when $\alpha = 90°$, we expect R_c to fall as the tilt increases[1]), and minimize ΔR_c over α to find the preferred mode. We find that $\alpha = 0$ is preferred for $\phi < B/2C \equiv \phi_c$, and $\alpha = \cos^{-1}(\phi_c/\phi)$ for $\phi > \phi_c$.

In other words, perpendicular rolls are preferred for small ϕ, and oblique rolls are preferred for larger ϕ. The transition between the two occurs at $\phi = \phi_c = B/2C$, and we will refer to this point as the 'Lifshitz point' after a similar phenomenon in nematic liquid crystals (see e.g. Silber et al., 1992).

For this model to be useful we require ϕ_c to be small; if not, then the assumption of small ϕ would not hold, and the model would break down. However, in our actual numerical results we find that $B/2C$ is typically less than 0.1, so this is not really a problem.

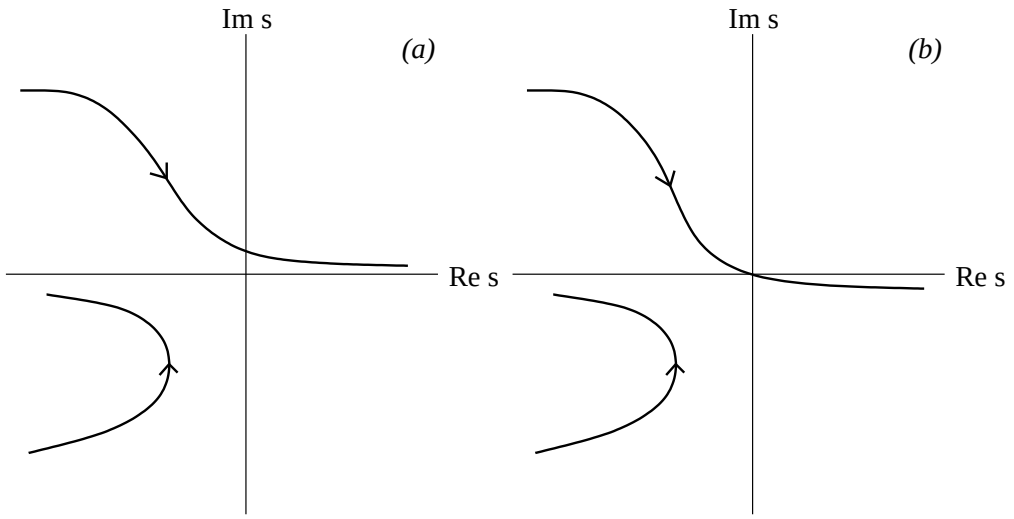

Figure 2.5: *The equivalent of Figure 2.3 for the steady case.*

2.4.3 The steady case

The above results have concentrated on the oscillatory case; the steady case (large ζ) is a little different. Note that the name 'steady' is slightly misleading, since the solutions are only truly steady if the field is vertical; this is illustrated in Figure 2.2(b), where the eigenvalues pass through the origin at $R^{(e)}$, indicating a steady-state bifurcation. As we shall see shortly, when the field is non-vertical the solutions do start to travel; the speed of travel is proportional to ϕ for small ϕ.

The perturbations to Figure 2.2, that would be expected in the steady case, are shown in Figure 2.5. This shows the path that the eigenvalues would take as R is increased, for a small non-zero ϕ. This is obtained by starting from Figure 2.2(b) and imagining a small perturbation that breaks the left-right symmetry – we are again assuming that we have found a suitable way of breaking the up-down symmetry in the layer. If the symmetry is only broken by changing the magnetic boundary conditions, then as discussed above, the curve must pass through the origin, so Figure 2.5(b) results; otherwise, we get Figure 2.5(a).

Notice that the eigenvalues in the right half-plane no longer remain purely real. In Figure 2.5(a), the curve crosses the imaginary axis at a non-zero value of $\mathrm{Im}\, s$, meaning that the bifurcation to convection is no longer a steady-state one, but an 'imperfect'

[1]When $\alpha = 90°$ (or equivalently, $k_x = 0$), we see from equations (2.15)–(2.23) that ϕ now only enters the problem in the combination $Q\cos\phi$. This indicates that increasing ϕ is equivalent to reducing Q, which in turn increases instability to convection and reduces R_c. We conclude that (when $\alpha = 90°$ at least) R_c must fall as the tilt increases.

bifurcation in which a small non-zero oscillation frequency (or equivalently, speed of travel) is present. Compare this to the oscillatory case in which the speed of travel is non-zero even when the field is vertical. In Figure 2.5(b), we do have a steady-state bifurcation at onset (the curve goes through the origin), but Im s still becomes non-zero for $R > R_c$.

Another difference between the steady and oscillatory cases is that in the former, the graph only crosses the imaginary axis once, indicating that waves can only travel in one direction (either leftwards or rightwards). This indicates that we could transform to a moving frame in which the pattern appeared to be steady. (Contrast this to the oscillatory case, where the graph crossed the imaginary axis at points both above and below the origin, indicating that both left-going and right-going waves could be present simultaneously, and no such Galilean transformation could be made.)

We now turn to the three-dimensional problem. In the oscillatory case, we noted above that one expects perpendicular rolls for small ϕ, and oblique rolls for large ϕ. This arose by considering the separate left-going and right-going perpendicular roll modes, and the symmetry breaking between them; this meant that ΔR_c for these modes was proportional to ϕ.

In the steady case, there are not separate left-going and right-going modes, and so the symmetry breaking does not apply; instead, ΔR_c for the perpendicular rolls is proportional to ϕ^2 (not ϕ as before). Also, the parallel rolls do not travel; since there is no reason for them to travel in either the positive or negative y direction, in the steady case they do not travel at all. Thus ΔR_c is proportional to ϕ^2 for the parallel rolls as well. So, without knowing the respective constants of proportionality (which cannot be obtained through simple symmetry arguments alone), we cannot say anything about which orientation of roll is going to be preferred in the steady case.

2.5 Results

2.5.1 Small ζ (oscillatory case)

Two-dimensional results ($k_y = 0$)

In this section, we give the results of our numerical solution of the eigenvalue problem described in section 2.2. The problem solved is exactly the one described in that section, with the following choice of parameters: $Q = 200$, $\zeta = 0.1$, $\sigma = 1$. (However, we do

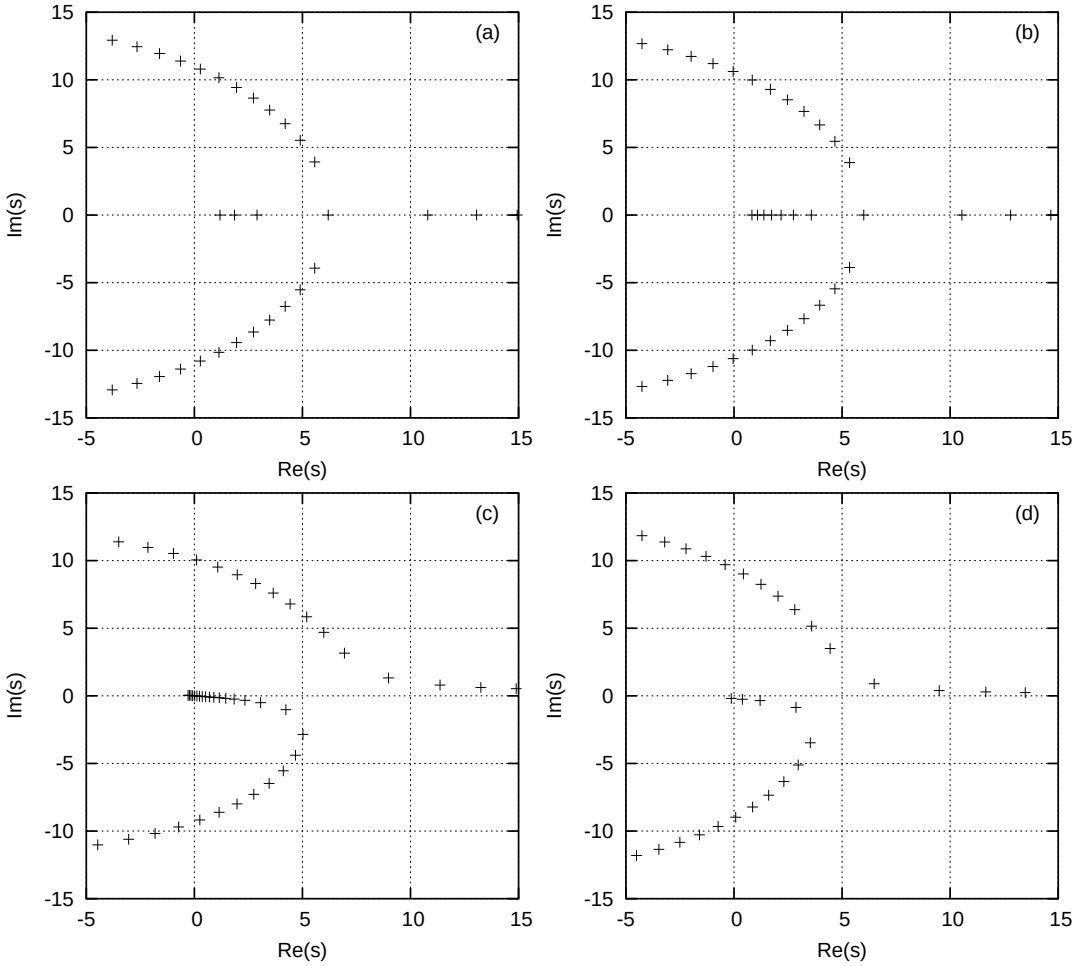

Figure 2.6: *Plots of eigenvalues s in the complex plane as R is varied. The crosses are plotted at intervals of 200 in R. In each case $\boldsymbol{k}$ is fixed and equal to $(k_c, 0)$, where k_c is the critical wavenumber (i.e. the one that minimizes R_c). (a) Vertical field ($\phi = 0°$), with $\hat{\kappa} = 1$. (b) $\phi = 15°$ and $\hat{\kappa} = 1$. (c) As (b), but with a fixed angle condition at the bottom of the layer (the other three cases use a tied field condition at the bottom.) (d) $\phi = 15°$ and $\hat{\kappa} = (z + 1/2)^{-3}$. Note: in case (c) the locus of eigenvalues passes through the origin, whereas in case (d) it merely passes very close to the origin – it in fact crosses the imaginary axis slightly below the origin.*

not find any significant qualitative difference for different choices of parameters, except for the change between oscillatory and steady behaviour as ζ varies.) The magnetic boundary conditions are to match onto a potential field above the layer, and to have a perfectly conducting lower boundary (as discussed in section 2.2), except where stated otherwise below.

Figure 2.6(a) shows a plot of the eigenvalues in the complex plane for a typical case with a vertical magnetic field. As expected on symmetry grounds, the eigenvalues come in complex conjugate pairs, showing that there is no preference for either left-going or right-going waves (cf. Figure 2.2a). Figure 2.6(b) shows the same situation but with ϕ increased to 15°. In this case a diagram similar to Figure 2.3(b) is expected, as explained above. Surprisingly, however, the eigenvalues still come in conjugate pairs, and the left-going and right-going waves still have identical growth rates (at any given Rayleigh number)!

This unexpected result is apparently a consequence of our particular choice of boundary conditions. For example, when using a fixed-angle condition at the bottom (instead of the 'tied field' condition), but keeping the potential field condition at the top, Figure 2.6(c) results. (A similar graph is also obtained if one uses a tied field at one surface with a fixed angle condition at the other.) Therefore, it appears that the left-right symmetry is not *always* broken by choosing different magnetic boundary conditions at top and bottom; apparently it sometimes is and sometimes isn't, depending on precisely which boundary conditions are chosen.

This is unfortunate since, as discussed above, the whole point of introducing the different boundary conditions at top and bottom was to try to break this symmetry. Of course, we could abandon our preferred choice of boundary conditions (Figure 2.6(b)), and use a combination that does break the symmetry (e.g. Figure 2.6(c)). However, we have argued that the fixed-angle condition is unphysical, and we prefer not to use it.

At this point, therefore, we bring in our alternative method of breaking the symmetry: a non-uniform thermal diffusivity κ. This is not unreasonable since in the Sun, the thermal diffusivity decreases as a function of depth, due to hydrogen ionization effects (Meyer et al., 1974). The profile $\hat{\kappa} = (0.5 + z)^{-3}$ was chosen. (In fact, the precise choice of this function does not make much qualitative difference; any monotonically decreasing function seems to give similar results.) Figure 2.6(d) shows the path of the eigenvalues that is now obtained. As expected, the left-right symmetry is broken, and the left-going waves are preferred (in this case). (If we 'reverse' the choice of κ, so that

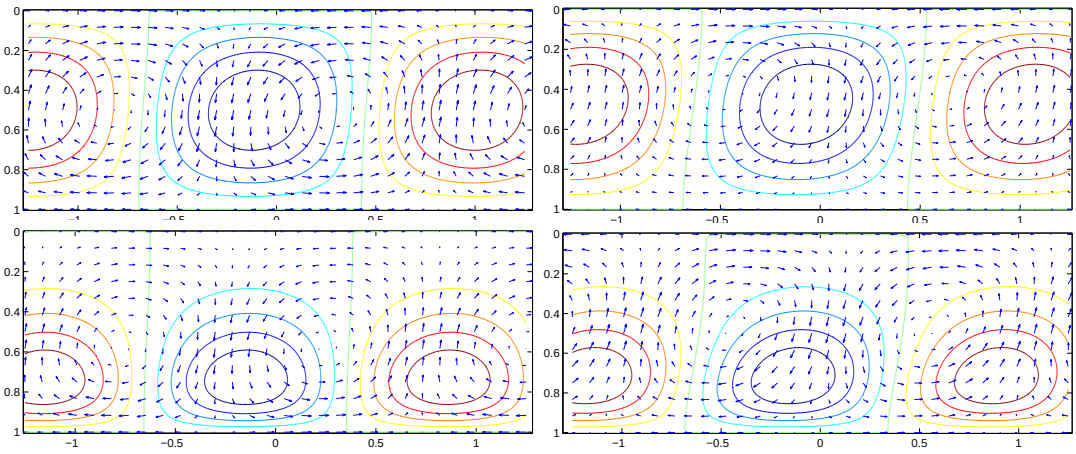

Figure 2.7: *Plots of the solutions obtained, with $\phi = 45°$. The contours show the temperature perturbation, and the arrows show the fluid velocity. The top two plots have $\hat{\kappa} = 1$ while the bottom two have $\hat{\kappa} = (1/2 + z)^{-3}$. The left panels show the left-travelling waves, while the right panels show the right-going solutions.*

it increases rather than decreases with depth, then the preferred direction of travel is to the right – as might be expected.)

Figure 2.7 shows some of the solutions themselves. These are produced by multiplying the eigenfunctions by $\exp(\mathrm{i}kx)$ and plotting the real part of the result (as explained earlier). The upper two panels show the solutions when κ was chosen to be uniform; note that these are not simply mirror images of each other, so the symmetry π has indeed been broken here, even though the growth rates (and critical Rayleigh numbers) for these two solutions are, for whatever reason, identical. In the bottom two pictures, in which κ varies with depth, this is no longer the case. Notice that the temperature perturbation is now concentrated towards the bottom of the layer; this is because heat is being transported more by conduction near the surface, where the heat conductivity is greater, and more by convection at the deeper levels, where the conductivity is lower.

Figure 2.8 shows the variation of the critical Rayleigh number with wavenumber. The first plot shows the vertical field case, in which the oscillatory mode is preferred when it exists (for k_x sufficiently small). The second plot shows what happens when the field is inclined; the preference for left-going waves is clearly visible. Note that the right-going wave has two critical Rayleigh numbers for each wavenumber; this is because the eigenvalue crosses the imaginary axis twice as R changes (see Figure 2.6d). The lower of these two values is the physically relevant one.

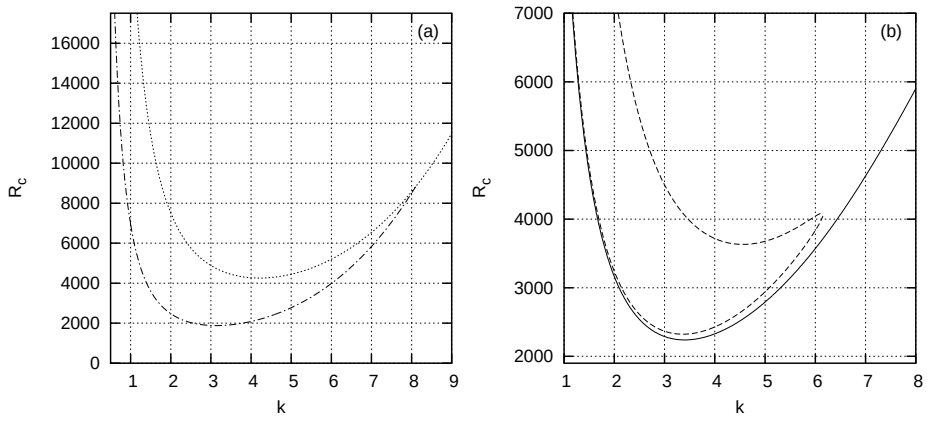

Figure 2.8: *R_c as a function of k_x. (a) Vertical field. We obtain both steady solutions (dotted curve) and oscillatory solutions (dash-dotted curve). (b) Tilted field ($\phi = 10°$). Here all solutions travel, either leftwards (solid curve) or rightwards (dashed curve).*

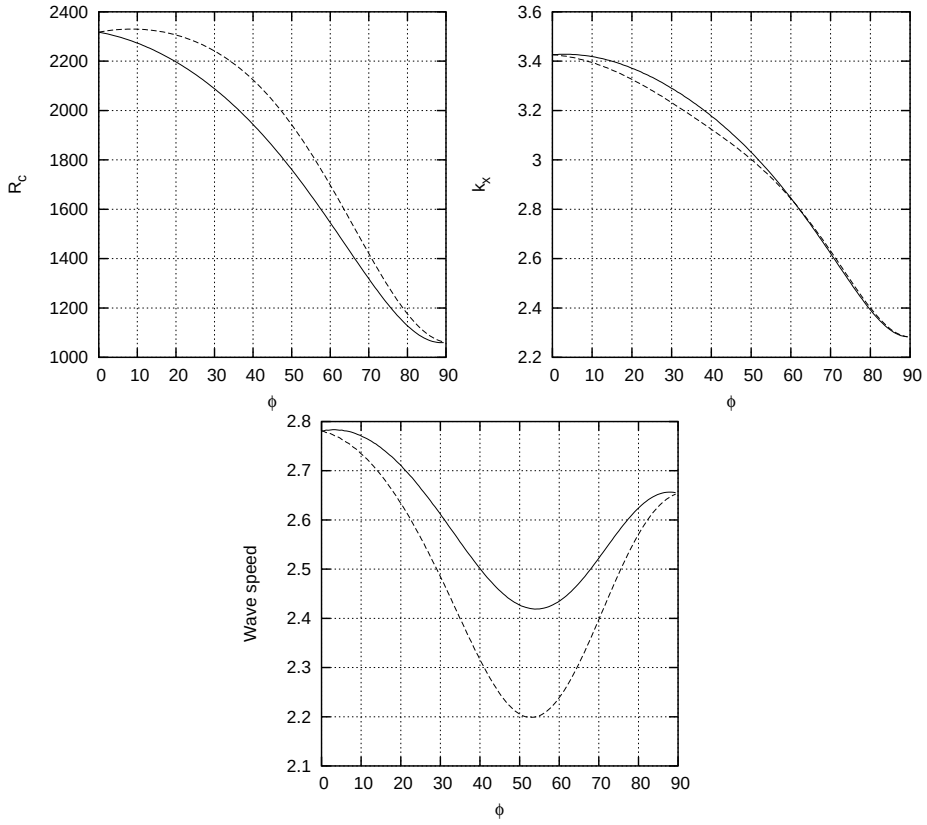

Figure 2.9: *Graphs of the critical Rayleigh number (R_c), the wavenumber (k_x) and the wave speed, as functions of ϕ.*

Figure 2.9 shows how R_c, k_x and the wave speed vary as a function of the tilt angle ϕ. These graphs confirm that the perturbations to each quantity are proportional to ϕ for small ϕ, as expected on symmetry grounds (see previous section). This applies for ϕ up to about 5–10°. After this point, the critical Rayleigh number decreases for both left- and right-going waves. Note also that the wavenumber decreases (equivalently, the wavelength increases) with increasing tilt, indicating that the solution is being stretched out along the tilt direction. This is understandable in that one would expect the convection cells to try to align themselves with the magnetic field lines, and this would cause them to appear to stretch out along the tilt direction.

Three-dimensional results

So far our results have been restricted to the two-dimensional case with $k_y = 0$; we now move on to three-dimensional solutions. To clarify, we are at this point continuing to use our depth-dependent profile for $\hat{\kappa}$, which, as mentioned above, is sufficient to break the symmetry between the leftward- and rightward-travelling modes.

Figure 2.10 shows contour plots of R_c as a function of both k_x and k_y for four different tilt angles. (Note that the convention that we have used is that left-going waves are plotted for k_x negative, and right-going waves are plotted for k_x positive.[2]) The preferred mode corresponds to the point in $\boldsymbol{k}$-space that minimizes R_c; this point has been marked by an asterisk on each diagram. Figure 2.11 shows the angle α (as defined in equation 2.41) corresponding to the preferred mode. This shows clearly which type of roll (from Figure 2.4) is preferred at each ϕ; $\alpha = 0°$ corresponds to perpendicular rolls, $\alpha = 90°$ represents parallel rolls, while an α in between these two values means that oblique rolls are preferred. Finally, Figure 2.12 shows the critical Rayleigh number for the different types of rolls as a function of ϕ.

Figures 2.10 and 2.11 are related, in that the position of the minimum on Figure 2.10, for a given ϕ, determines the value of α corresponding to that ϕ on Figure 2.11. Hence, we see that the minimum is located on the negative k_x axis for the smallest ϕ values (Figure 2.10a), which means that α is zero for small ϕ. When ϕ reaches a critical value (just above 10° in this case), the minimum leaves the k_x axis and moves

[2]Effectively what we are doing here is demanding that Im s be negative, and then using the sign of k_x to indicate the direction of travel. This is in contrast to our previous figures where k_x is assumed positive and the sign of Im s was used to indicate the direction of travel. The two are of course equivalent; this can be seen from equations (2.11)–(2.14), which remain invariant if one changes $\boldsymbol{k}$ to $-\boldsymbol{k}$ and s to $-s$.

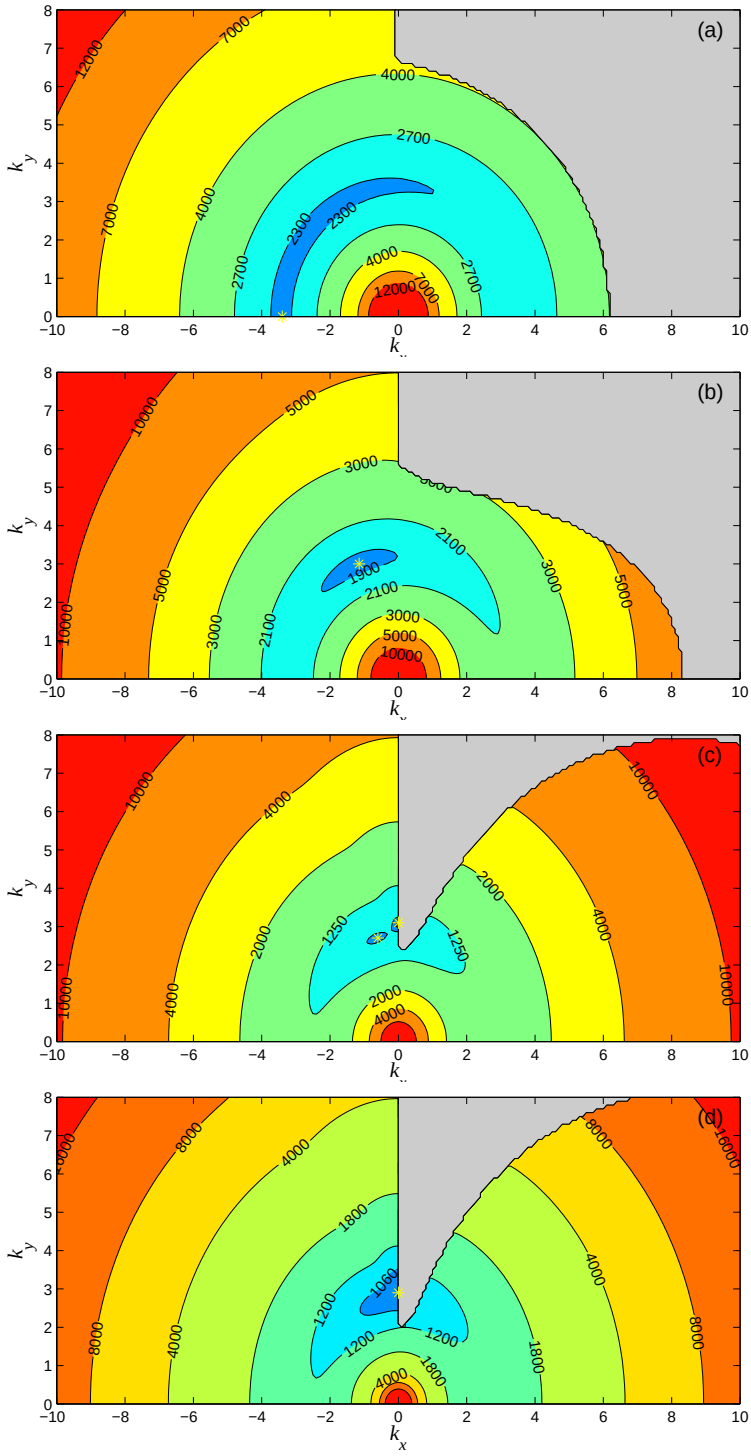

Figure 2.10: *Contour plots showing critical Rayleigh number as a function of wavevector, with positive (negative) k_x representing right-going (left-going) waves. The shaded areas represent regions where no right-going solution exists. The preferred mode (corresponding to the minimum R_c) is indicated by a small asterisk in each plot. The four cases are (a) $\phi = 10°$, (b) $\phi = 40°$, (c) $\phi = 72.5°$, (d) $\phi = 75°$.*

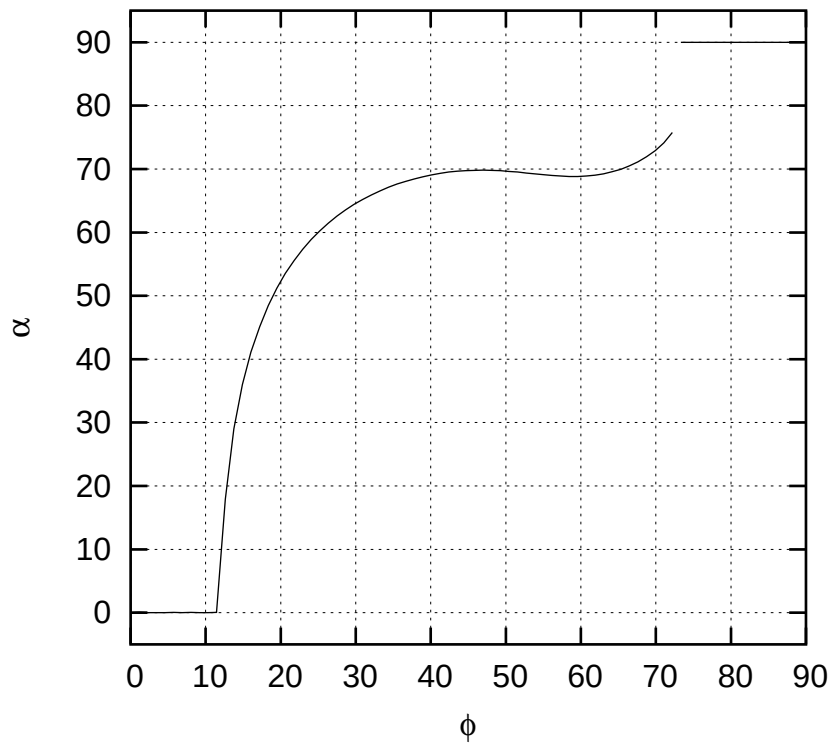

Figure 2.11: *The preferred orientation α of the convection rolls as a function of ϕ.*

up and to the right. This is quite rapid at first and is visible as a sharp increase in α on Figure 2.11. Physically, this means that the preferred mode has changed from being perpendicular rolls to being oblique rolls. Indeed this transition is the same as the one predicted by symmetry arguments (section 2.4.2). By $\phi = 40°$ (Figure 2.10b) the minimum has settled to a position corresponding to $\alpha \approx 70°$. For larger ϕ, a second local minimum appears on the positive k_y axis; this is not initially the lowest of the two minima, but it rapidly decreases in value and eventually 'overtakes' the original minimum to become the new global minimum. This results in a discontinuous change in α and is the reason for the discontinuity in Figure 2.11. The point where the minima 'cross' can be seen in Figure 2.10(c). For higher values of ϕ the parallel rolls are now dominant (Figure 2.10d).

This behaviour can be compared to the predictions of the simple model from section 2.4.2, and in particular, equation (2.42). As already stated, the main prediction was that there would be a transition from perpendicular to oblique rolls, and this transition was expected to occur at $\phi = B/2C$ where B and C are as defined in (2.42). The values of B and C can be estimated by inspecting the numerical results near $\phi = 0$; we find $B = 163.6$ and $C = 923.2$, which gives $B/2C = 0.089$ radians, or 5.1 degrees, which is

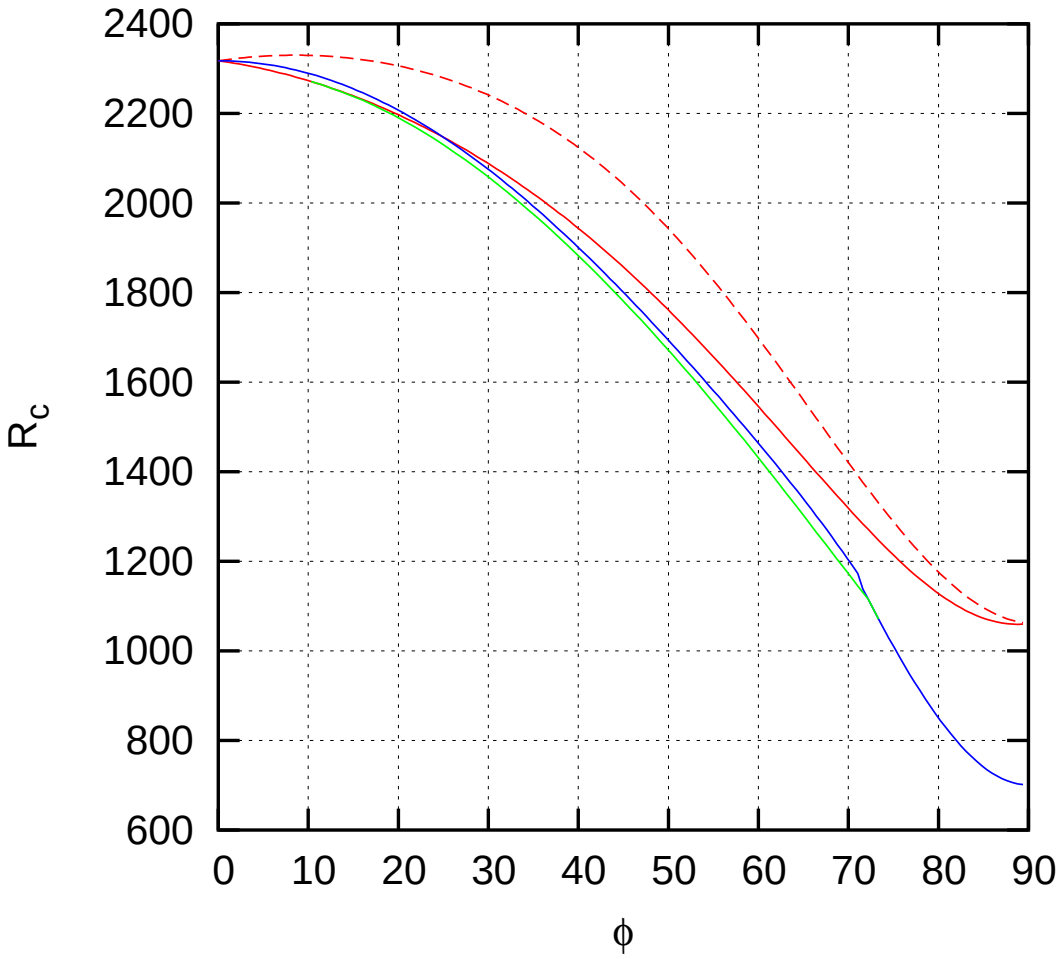

Figure 2.12: *The critical Rayleigh numbers R_c for various modes as a function of ϕ. The colour coding is the same as in Figure 2.4. The red curves show critical Rayleigh numbers for perpendicular rolls, corresponding to our two-dimensional solutions; the dashed curve is for the right-going rolls, and the solid curve is for the leftward-travelling solutions. The blue curve is for parallel rolls, and the green for oblique (more precisely, the green curve shows the critical Rayleigh number for the most unstable oblique mode, when such a mode is more unstable than either the perpendicular or parallel rolls).*

about a factor of two too small (compared to the actual location of the Lifshitz point). Therefore, the model equation (2.42) is accurate qualitatively but not quantitatively, although the latter is hardly surprising given the ad hoc nature of the model (e.g. the factors of $\cos\alpha$ and $\sin\alpha$ were invented in order to satisfy the right properties, rather than to be an exact quantitative description).

One thing that the model equation (2.42) does get wrong, even qualitatively speaking, is that it does not predict the discontinuous jump in α, and the associated appearance of a second local minimum in R_{c}, which occurs for larger values of ϕ. Therefore, we need to explain why this second minimum appears.

We can do this by considering the governing equations when $\alpha = 90^\circ$. In this case the horizontal component of the imposed field disappears from the equations, and this mode sees only the vertical component. As the tilt of the field increases, the vertical component of the field decreases and so the effective Chandrasekhar number decreases. Beyond a certain tilt the effective Q becomes too small for the oscillatory instability, and the mode becomes steady. This is the fact that was missing from the analysis of section 2.4. The critical Rayleigh number falls more quickly after this point (this is visible on Figure 2.12 as a 'kink' in the curve for parallel rolls, near $\phi = 70^\circ$) and the steady parallel mode soon becomes the dominant one.

The preference for parallel rolls for large ϕ is consistent with the work of Danielson (1961), who showed that in a *horizontal* magnetic field ($\phi = 90^\circ$), convection would consist of parallel rolls. Essentially, this is because this form of motion can just bodily displace the field lines, without distorting them; perpendicular or oblique rolls would have to twist the field lines, and this would be resisted by the Lorentz force.

One final point concerning Figure 2.10 is the meaning of the grey, shaded areas on the contour plots. (Note that the jagged appearance of these regions is not real, but is due to limited resolution.) These regions arise because, for certain wavevectors, no right-going wave exists, only a left-going one. This can be seen clearly on Figure 2.8(b), for example, where the right-going branch (the dashed curve) does not extend to values of k_x greater than about 6.

It is also of interest to consider what happens to the position of the Lifshitz point as the amount of up-down asymmetry (as determined by the choice of κ) is varied. To investigate this, we set $\kappa = (0.5 + z)^{-\kappa_0}$, and then plotted the value of ϕ corresponding to the Lifshitz point as a function of κ_0; see Figure 2.13. It can be seen that as the amount of up-down asymmetry is increased (corresponding to larger values of κ_0), the

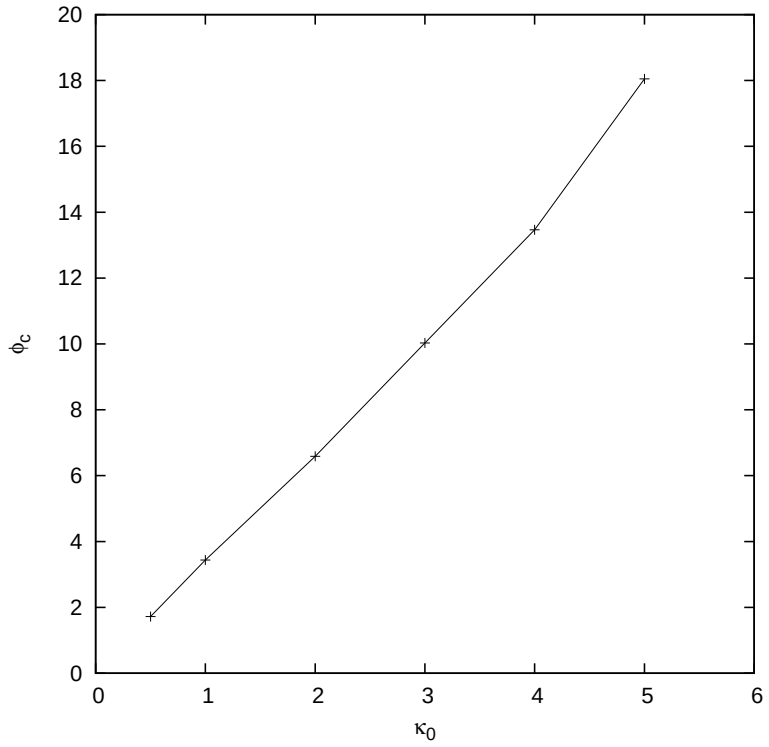

Figure 2.13: *The variation of ϕ_c (the value of ϕ corresponding to the Lifshitz point, measured in degrees) with κ. Here $\kappa = (0.5 + z)^{-\kappa_0}$ and κ_0 has been allowed to vary. (Other parameters: $Q = 300$, $\zeta = 0.1$, $\sigma = 1$.)*

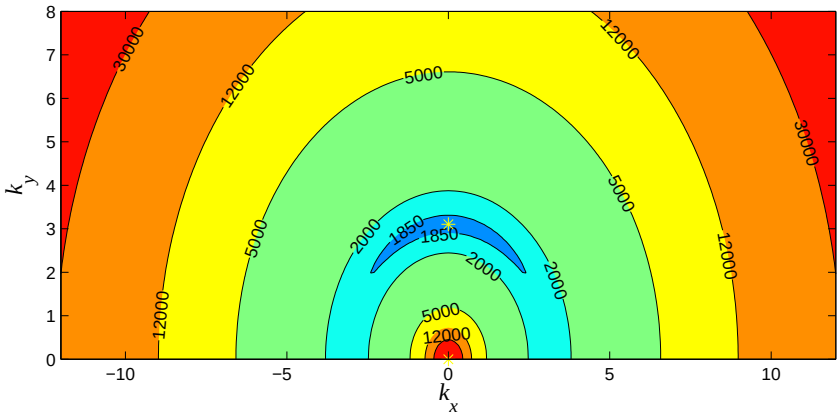

Figure 2.14: *Contour plots of R_c as a function of wavevector in the case where $\hat{\kappa}$ does not vary with depth. The tilt angle $\phi = 15°$. Notice that although these results are anisotropic, they are still left-right symmetric. This shows that the left-right symmetry, found in the two-dimensional results above, continues even when $k_y \neq 0$.*

Lifshitz point occurs at larger and larger values of ϕ.

For completeness, we also present the three-dimensional results for the case where $\hat{\kappa}$ does *not* vary with depth. (Recall from the previous section that in this case, the left-right symmetry is *not* broken, despite expectations to the contrary.) The contour plot of R_c against k_x and k_y is shown in Figure 2.14. Notice how this unexpected left-right symmetry persists even when $k_y \neq 0$.

2.5.2 Steady case

The results here are actually a little simpler than the oscillatory case, and so less space will be devoted to these. As noted above, the solutions are expected to start travelling as soon as ϕ increases above zero, but we cannot say from symmetry arguments which direction the solutions will travel in. Nor can we say in advance which of parallel, perpendicular, or oblique rolls will be preferred.

In order to obtain a steady, rather than oscillatory, bifurcation (when $\phi = 0$), we have taken $\zeta = 1.1$ instead of 0.1 in this section (leaving the other parameters unchanged). We are also using the depth-dependent profile for $\hat{\kappa}$ in this section.

A contour plot of R_c against k_x and k_y, for the case $\phi = 45°$, is shown in Figure 2.15. Note that in this case, all solutions travel to the left (i.e. against the tilt), and no solutions travel to the right; consequently, the figure only shows results for $k_x < 0$.

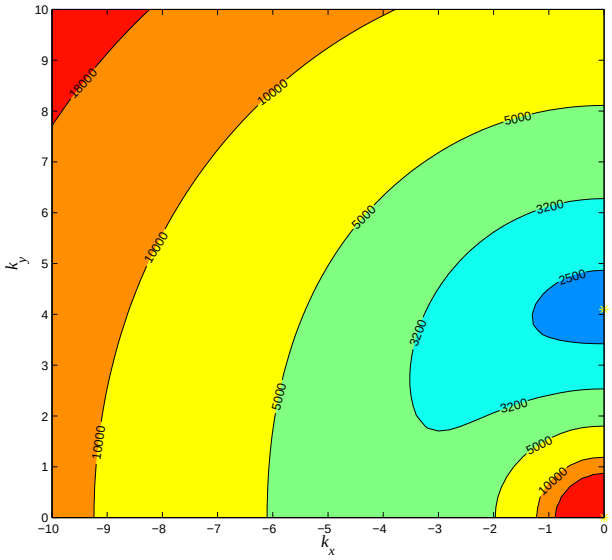

Figure 2.15: *Contour plot of R_c against k_x and k_y in the steady case. Note that all solutions travel leftwards (or else are steady), hence only the left-hand half of the diagram is shown.*

Notice how the anisotropy introduced by the tilt is clearly visible. The minimum R_c occurs on the k_y axis, indicating that parallel rolls are preferred. In fact, we find that parallel rolls are the preferred mode for all ϕ in this case.

In Figure 2.16 we plot R_c, the wavenumber and the wave speed as functions of ϕ, for both parallel and perpendicular rolls. As regards the wave speed, this is zero for the parallel rolls (this is just because of the $y \to -y$ reflection symmetry), but it is non-zero for perpendicular rolls (and in fact oblique rolls as well). Note how the speed of travel is proportional to ϕ for small ϕ, as expected (indeed, this is true up to quite large ϕ, about 60° or so).

We can also compare our results to those of Chandrasekhar (1961) who briefly considered convection in inclined fields in the steady (large ζ) case. He also found that parallel rolls (with $k_x = 0$) would be the preferred mode for all ϕ. However, his model was purely Boussinesq, with uniform κ and identical boundary conditions at top and bottom. Therefore, his model contained the up-down symmetry that we talked about in the previous section, and so his solutions did not travel at all. By contrast, all our solutions (except the parallel rolls) travel to the left. This may seem irrelevant, since the preferred mode is the parallel rolls, which do not travel. However, once we move on to nonlinear solutions, all modes will be present in some sense, and we might expect to start to see the effects of the travelling modes.

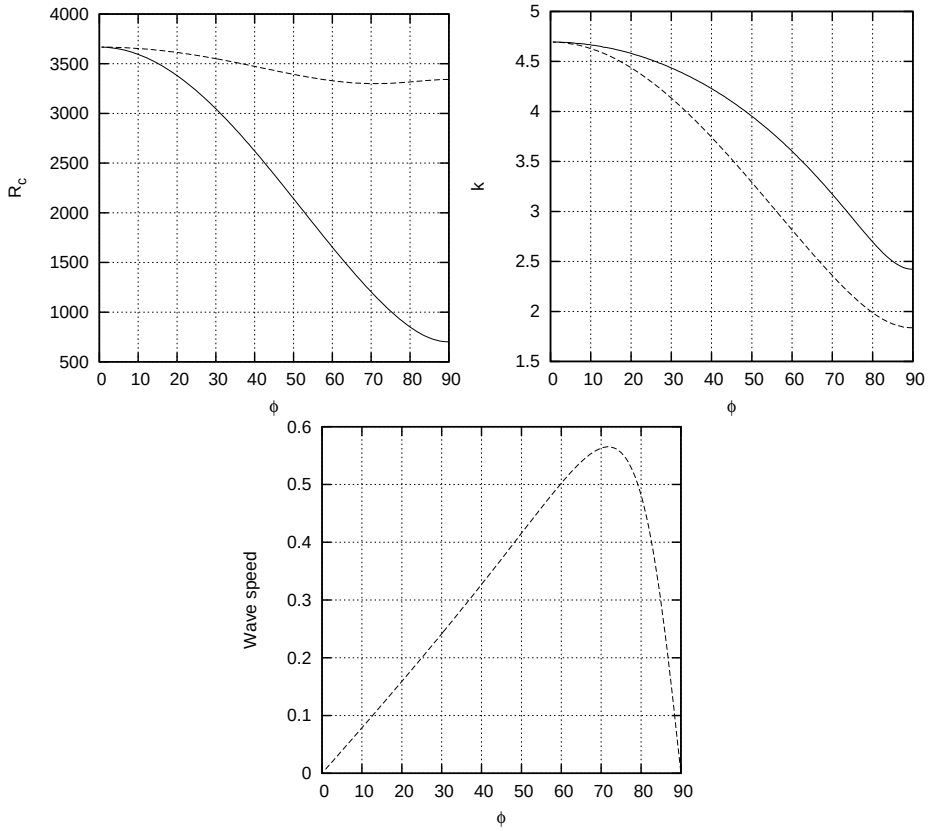

Figure 2.16: *Graphs of the critical Rayleigh number (R_c), the wavenumber ($|\boldsymbol{k}|$) and the wave speed, as functions of ϕ. The solid line is for parallel rolls, while the dashed line is for perpendicular rolls.*

2.6 Conclusions

In this chapter we have investigated the linear stability theory for magnetoconvection in a Boussinesq fluid layer with an inclined magnetic field and a depth-dependent thermal diffusivity κ.

We included the depth-dependent κ as a way of breaking the up-down symmetry of the fluid layer, a symmetry that is present in Boussinesq but not in compressible convection. Since compressibility is important in sunspots, it was important to find a way to break this symmetry in our model. We at first tried to do this simply by modifying the boundary conditions at the top and bottom of the layer, but that was found to be unsatisfactory (for reasons explained above), and so we included the depth-dependent κ instead.

The most important effect of tilting the field is that the layer becomes anisotropic, so that rolls of different orientations have different stability properties, and modes can now exhibit a preferred direction of travel (either towards or away from the tilt direction).

When ζ is large (the 'steady' case) the preferred mode is parallel rolls for all ϕ. These are steady, but rolls in any other orientation travel (with a speed proportional to ϕ for small ϕ). These travelling modes are not preferred near onset, but their presence suggests that patterns in the nonlinear regime might travel.

For small ζ (the 'oscillatory' case), the results are more complicated. In the two-dimensional problem ($k_y = 0$), we find broadly similar results to those of Matthews et al. (1992), with symmetry-breaking between left- and right-going modes. In the three-dimensional problem ($k_y \neq 0$), we find that travelling perpendicular rolls are preferred for small ϕ, travelling oblique rolls for intermediate ϕ and steady parallel rolls for large ϕ. Note that Matthews et al. (1992) predicted that the transition between perpendicular and oblique rolls would be found, but they did not predict the transition between oblique and parallel rolls for larger ϕ. This comes about because the vertical component of the magnetic field drops as ϕ increases, which triggers a change from oscillatory to steady convection.

Perhaps the main difference between our model and that of Matthews et al. (1992) is in the direction of travel of the preferred mode. We find waves travelling to the left (against the tilt) for all ϕ; they find waves travelling to the right for most ϕ, but for a small range of ϕ near 90°, this reverses and the waves travel to the left. They can also produce left-going waves for all ϕ by changing their boundary conditions. Clearly, the

direction, and speed, of travel are highly model-dependent. Nevertheless, in terms of application to sunspots, it is encouraging that some models, at least, show a reversal of direction of travel as ϕ increases – even if it is the wrong way around (in a sunspot, features are observed to move inwards, i.e. 'left', for small ϕ and right for large ϕ)!